Available online at www.sciencedirect.com

ScienceDirect

Ceramics International 40 (2014) 14483–14491

CERAMICS INTERNATIONAL

www.elsevier.com/locate/ceramint

Titanate nanotubes produced from microwave-assisted hydrothermal synthesis: Photocatalytic and structural properties

Daniela C. Manfroi[a,*], Ademir dos Anjos[b], Alberto A. Cavalheiro[b], Leinig A. Perazolli[a], José A. Varela[a], Maria A. Zaghete[a]

[a]Centro Multidisciplinar para o Desenvolvimento de Materiais Cerâmicos, Instituto de Química, UNESP, CP 355, 14801-907 Araraquara, SP, Brazil
[b]Centro de Pesquisa e Tecnologia em Recursos Naturais (CPTREN), UEMS 275, Emilio Mascoli street, 79950-000, Naviraí, MS, Brazil

Received 29 May 2014; received in revised form 24 June 2014; accepted 1 July 2014
Available online 10 July 2014

Abstract

Titanate nanotubes were successfully synthesized using the microwave-assisted hydrothermal method from commercial TiO_2-anatase powder. Several samples were obtained at varying temperatures and time. Powder samples containing titanate nanotube ($Na_2Ti_6O_{13}$) single phase were obtained at 130 °C for 4 h and 150 °C for 2 h, demonstrating the kinetics dependence of reaction temperature. Through XRD analysis and electron diffraction pattern, the nanotube structures were found to be composed of a short range ordering, thus giving rise to a broad XRD peak profile. The higher time and temperature (150 °C for 4 h) led to the formation of more organized structures. The nanotubes UV–vis spectra showed a band gap of 3.90 eV and a shoulder on the curve which led to another band gap value 3.25 eV. The photoluminescence spectrum emission peak presented a significant decrease, indicating the reduction of surface or structural defects of titanate nanotubes due to longer hydrothermal treatment duration. All structural, electronics and morphologics transformation led to an improvement on photocatalytic activities for nanotubes, especially the sample obtained at 150 °C for 1 h that rate of decolorization is 0.01879 min^{-1}, 2.25 times faster than TiO_2-anatase (starting phase).

Keywords: Microwave hydrotermal synthesis; Titanate nanotubes; Photoluminescence; Photocatalysis

1. Introduction

The increasing demand in materials exhibiting high surface areas for technological purposes such as adsorbents [1], sensors [2–4], photocatalysts [5,6], agriculture [7] and drug delivery [8,9] has led to innovative approaches for dioxide titanium (TiO_2) based materials. To this end and for attaining success in the above-mentioned applications, the need for more efficient materials with higher surface area cannot be over-emphasized. Chemical synthesis methods can also be used for this purpose, such as microemulsion technique [10], sol–gel [11], Polymeric Precursor [12], and Hydrothermal [13], as well as changes in synthesis parameters like temperature, time and pH, or the use of modifiers as carbon [14], nitrogen [15] and basic cations (Mg^{2+}, K^{+}, Ba^{2+}, Zn^{2+}) [16] wich led to improvement on materials properties. These approaches can enhance the morphological, mechanical, electric, optical and thermal properties of nanoparticles surfaces, including the development of 1D nanostructures, such as tubes, wires or needles [17]. Several synthesis routes have been studied since titanium nanotube synthesis was described for hydrothermal conventional method from the titanium oxide [18,19]. Other studies have also been conducted using similar methodology [20–22]. The effects of the concentration of NaOH on the structures and formation mechanisms of various titanate was presented in a detailed in a study and was found that the morphologies of the titanate products were determined by the concentration of NaOH [23]. Starting from titanium dioxide at low temperature, an effective 1D structure only occurs after about 20 h using the conventional hydrothermal method. Microwave as the heat source was found to reduce the reaction time to around 2 or 3 h, but a further reduction can be attained with an increase in temperature [24,25]. The parameters of the

*Corresponding author.
E-mail address: danimanfroi@hotmail.com (D.C. Manfroi).

http://dx.doi.org/10.1016/j.ceramint.2014.07.007
0272-8842/

microwave-assisted hydrothermal synthesis, such as reaction time and temperature, TiO_2 amount and power source of the equipment were studied in order to understand their influence on the process of obtaining nanowires. Results have shown that the temperature affects most notably the product morphology, while the treatment time affects the final length as well as the amount of nanowires[24]. Indeed, the structure–property correlation for these materials requires yet further investigations and the primary goal of this work is to investigate some of these aspects for the sodium titanate nanotube synthesis by the microwave-assisted hydrothermal method. This paper shows the influence of time and temperature on the sodium titanate nanotube synthesis as well as the variations in photoluminescence, electronic properties and photocatalysis activities as a consequence of the structure and morphology obtained.

2. Material and methods

2.1. Synthesis

The microwave-assisted hydrothermal method (MAH) was used to synthesize sodium titanate nanotubes. By using a digester CEM Corp. brand. (Matthews, NC), model-5 MARS set to 450 W in operating power, reagents which have not been previously purified were inserted into a closed Teflon® (XP-1500) vessel. A sodium hydroxide solution at concentration of 10 mol L^{-1} was prepared using NaOH pellets (Synth). Then 0.4286 g of TiO_2-anatase powder (VETEC) with particles size of about 100 nm was added to the previous solution in order to obtain a suspension volume of 50 mL. A number of synthesis conditions were investigated, varying the temperature from 130 to 200 °C and the time reaction from 30 min to 4 h. The powder samples obtained were washed with deionized water until the pH was stabilized to about 6.0 and were then dried at room temperature.

2.2. Samples characterization

All of the samples were morphologically and structurally characterized by X-ray diffractometry (XRD), Raman spectroscopy and scanning and transmission electron microscopy. For the XRD technique, a Rigaku 2000 diffractometer with monochromatic Cu Kα radiation at 2θ range of 10–80° with step of 0.01° was used. The particles morphology was investigated by scanning electron microscopy (SEM) on a JEOL FEG-SEM, JSM-7500F and Transmission Electron Microscopy (TEM) Philips CM 200. For the Raman spectroscopy characterization, a Bruker equipment RFS100/S with a Nd:YAG laser providing an excitation light at 1.064 with a spectral resolution of 2 cm^{-1}, in the range 1100–20 cm^{-1} and 64 scans was used. The photonic characteristics were analyzed by UV–vis diffuse reflectance using a Cary spectrophotometer UV–vis NIR and 500 by MgO as a reflectance standard in order to calculate the band gap values. Besides that, the photoluminescence spectra were collected through a Thermal Jarrel-Ash monochromator Monospec 27 and a Hamamatsu R446 photomultiplier, with wavelength of 350 nm for excitation of krypton laser ions (Coherent Innova) with power maintained at 550 mW.

Photocatalytic studies were carried out using 100 mg L^{-1} of TiO_2-anatase and nanotubes sample dispersed in 500 mL of 0.01 mmol L^{-1} aqueous solution of rhodamine-B. The suspended solution was stirred a few minutes in the dark and then it was put under a Phillips germicide lamp (254 nm). Degradation was monitored by taking aliquots at increasing time intervals. These aliquots were filtered with Millipore® (0,45 μm) membranes and then tested using a UV–vis Femto Cirrus 80PR spectrometer to get the absorption spectra. The concentration curve was obtained by max rhodamine-B absorbance peak (554 nm). The rate of degradation was obtained according to Eq. (1):

$$\ln\left(\frac{A_0}{A}\right) = kt \quad (1)$$

where A_0 is the initial absorbance, namely, after stirred a few minutes in the dark, and A is the characteristic absorbance peak at degradation for a time, t.

3. Results and discussion

The XRD patterns for the powder samples obtained by MAH at 130 °C, 150 °C, 180 °C and 200 °C for varying reaction times (0.5–4 h) are shown in Fig. 1. For a temperature of 130 °C (Fig. 1a), the anatase phase (A), which is the single one in the starting powder remains highly crystalline with the time of reaction in spite of its rapid consumption toward the formation of the nanotube phase (✻). The anatase TiO_2 phase was identified following its comparison with JCPDS card no. 21-1272, which possesses space group I41/amd and lattice volume of 136.26 $Å^3$. Through the Rietveld refinement mechanism using structural model found in ICSD database (card no. 200392), the anatase phase in the starting powder was found to have a and c lattice parameters of 3.7848 and 9.5119 Å, respectively.

The sodium titanate nanotube formed in the reaction presents to a large extent very broad peaks both to the excessive peak overlapping and to the small nanometer size dimensions of the tubes. The main peaks are localized at $2\theta = 24$, 28 and 48° and the most intense one at $2\theta = 10°$, which can be related to these nanostructures, that have originated from titanate interlayers. In Fig. 1 it is possible to see that the difractograms start at $2\theta = 10°$, except for sample obtained at 180 °C (Fig. 1c) which starts at $2\theta = 5°$ and shows these peaks profile clearly. From these peaks profiles there are several possible structures, such as $Na_2Ti_2O_5 \cdot H_2O$, $H_2Ti_4O_9 \cdot H_2O$ or the lepidocrocite titanate $Na_xH_{2-x}Ti_3O_7$, and $H_2Ti_2O_4(OH)_2$, the non-washed hydrated titanic acid $H_2Ti_2O_5 . H_2O$ and the sodium trititanate nanotube ($Na_2Ti_3O_7$) as reported in the literature [26–29]. However, following a series of attempts to refine them all including the other ones, it was noted that the structure that exhibited the best adjustment corresponded to the composition $Na_2Ti_6O_{13}$ and C2/m

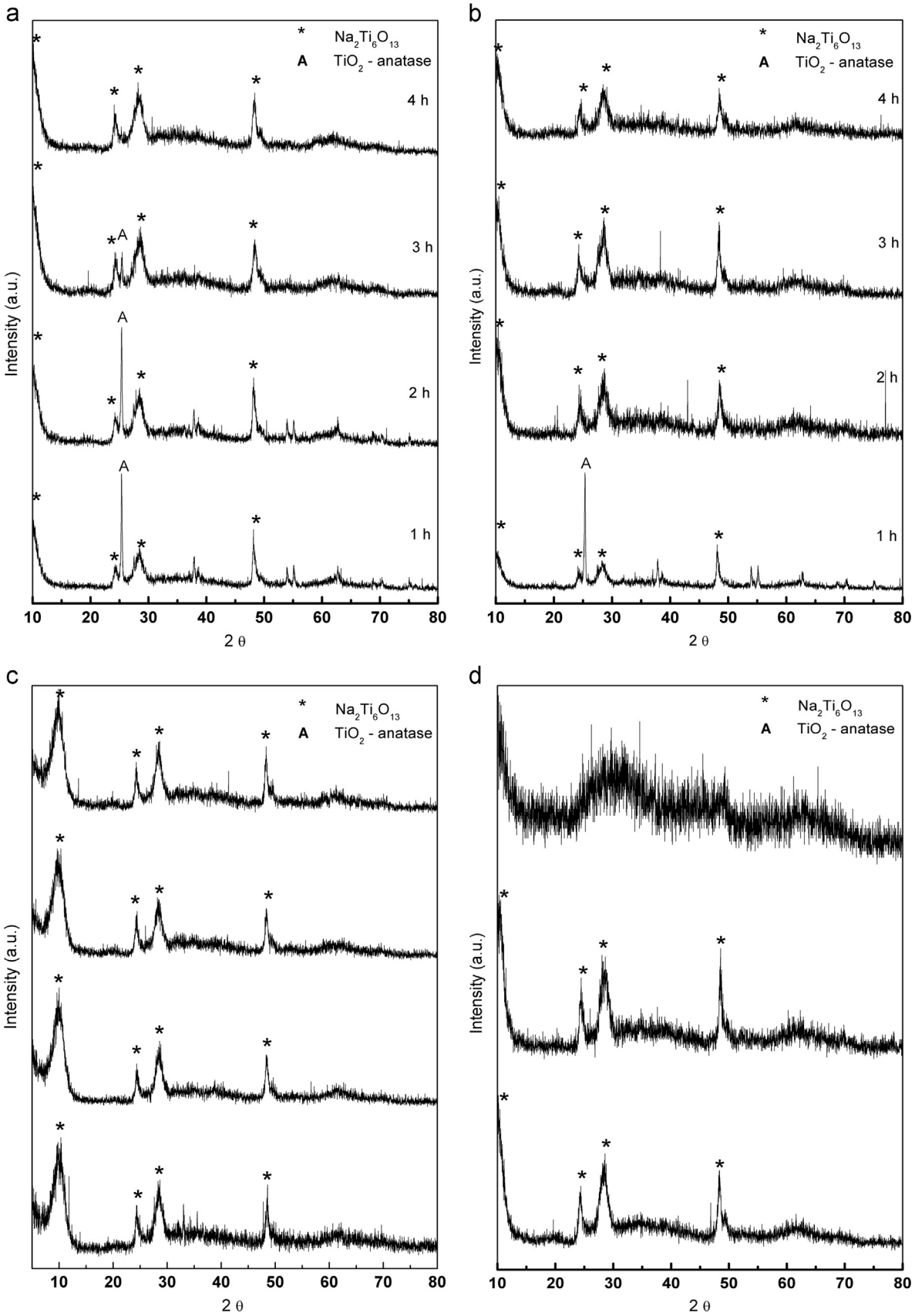

Fig. 1. XRD patterns for powder samples obtained from 0.5 to 4 h by MAH assisted at (a) 130 °C, (b) 150 °C, (c) 180 °C and (d) 200 °C (A = TiO_2-anatase phase; * = $Na_2Ti_6O_{13}$).

monoclinic space group, a finding which has not yet been reported elsewhere.

This observation is based on the Rietveld refinement mechanism as the monoclinic C2/m sodium titanate nanotube $Na_2Ti_6O_{13}$ with structural model found in ICSD database (card no. 1962) presented the lowest derived *R–F* (6.3) and a goodness-of-fit of 1.2. The other structure investigated by the refinement method does not reach derived *R–F* values lower than 18 and goodness-of-fit lower than 4, thus making the monoclinic C2/m sodium titanate nanotube $Na_2Ti_6O_{13}$ phase the most probable structure.

With regard to the $Na_2Ti_6O_{13}$ phase, the original lattice volume was 512.18 $Å^3$, but for the refined structure, this value rose to 637.44 $Å^3$. A comparison of the lattice parameters indicated the presence of an isotropic stretching in *a*, *b* and *c* lattice parameters. However, both the anatase and sodium titanate nanotubes $Na_2Ti_6O_{13}$ phases do not change significantly during the reaction, indicating that the process occurs by the dissolution–precipitation process, regardless of the synthesis temperature.

At 130 °C, the quantitative phase analysis shows a moderate anatase phase lixiviation, presenting a residual anatase phase of 65 mol% for 1 h. After 2 h, the residual anatase phase decreases to 50 mol% and to 25 and 8 mol% following 3 and 4 h of reaction respectively. Despite the fact that the anatase peak intensity for 2 h does not seem feasible once compared to the sample obtained after 1 h of reaction, the sodium titanate nanotubes peak profile undergoes a change in order to obtain different pondered phase amount. It is only after 3 h of reaction that the anatase particle consumption is significant enough to reduce the peak intensity while the anatase starting phase completely disappears in XRD pattern after 4 h of reaction.

By raising the temperature to 150 °C (Fig. 1b), the initial amount of anatase phase which was 50 mol% was found to decrease to 12 mol% after 2 h. Following 3 h of reaction, the anatase phase was found to be totally consumed and the same result was detectable for higher temperatures, such as 180 and 200 °C (Fig. 1c and d, respectively), even at the shortest reaction time. From these considerations we conclude that the transformation process by dissolution–precipitation undergoes the direct influence of temperature, reducing the time of processing.

Comparing the structural information obtained by XRD patterns with the morphological analysis obtained using SEM characterization (Fig. 2), it is possible to affirm the existence of a sequence of nanotube formation for both temperatures (130 °C and 150 °C). The sequence as can be seen in Fig. 2a–c from the SEM images, for synthesis reaction at 130 °C, that shows that the titanate nanotubes (Fig. 2b) are formed and they are found to grow by consuming the anatase starting particles (Fig. 2a). This mechanism results in specific hybrid morphology during intermediate stages and after 4 h of reaction the tubes become very long and coiled as seen in Fig. 2c. On the other hand, the titanate nanotubes are formed quickly at 150 °C, and even at a short time of reaction (1 h) the nanotube is found to be predominant in the sample, where some small TiO_2-anatase particles found remaining are dispersed into the nanotube matrix (Fig. 2d). Although after 4 h of reaction (Fig. 2e), the anatase starting phase is found to be already entirely consumed while the nanotubes are found exhibiting thicker walls, the sample however yet presents 1D morphology.

Taking into account the results obtained by conventional hydrothermal synthesis, using either commercial P25 or sol–gel synthesized TiO_2 powders in NaOH 10 mol L^{-1} aqueous solution favors nanotubes formation [5]. The proposed mechanism is composed of two mains steps: the first of which involves the dissolution of the TiO_2 particles by OH^- groups in order to form ultrathin titanate nanosheets, where the TiO_6 octahedrons are found in edge sharing. In the second step, the formed ultrathin nanosheets become folded in the form of short nanotubes through the dissolution–precipitation process, thus leading to their increase in length and wall thickness [9]. For higher temperatures, specifically at 180 and 200 °C, the reaction rate is increased significantly. After 1 h of reaction at 180 °C or 0.5 h at 200 °C, the complete anatase starting particles are consumed and the sodium titanate nanotube appears as a single phase.

By analyzing the particle structure using High Resolution Transmission Electron Microscopy (HRTEM), including the Electron Diffraction Pattern Analysis inset, it was possible to demonstrate that the nanotubes exhibit low-crystallinity type nanostructures, as can be observed in the XRD pattern (Fig. 1) due to a large extent to the broad peaks. The samples obtained at 130 °C and 150 ºC following 4 h of reaction are illustrated in Fig. 3(a) and (b), which proves that the material is composed of nanotubes with inner pore diameter of 3.5 nm. These HRTEM images suggest the presence of a different number of walls on opposite sides of the nanotube, depicting a scroll-like structure. The interlayer spacing for all of the samples is very close to 0.70 nm, but these multiwall-structured nanotubes have different outer diameters depending on the synthesis conditions. For the sample obtained at 130 °C for 4 h, the nanotubes are thinner and present an outer diameter of 11 nm, whereas the sample obtained at 150 °C after 4 h of reaction exhibited nanotubes with an outer diameter of 20 nm.

For lower temperature (130 °C), the nanotubes electron diffraction pattern shown in the figure inset (Fig. 3a) indicates the predominance of concentric rings associated to the low crystallinity material. This result is in line with the XRD pattern for this sample due to the broad peaks (Fig. 1a). When the temperature was increased to 150 °C (inset Fig. 3b), the figure showed concentric rings with the presence of some points of light indicating that the external thicker walls are more crystalline which reinforce the idea that the mechanism of nanotube formation is by dissolution–precipitation [30]. In addition, these samples were also analyzed by Raman spectroscopy (Fig. 4), the results of which demonstrate the presence of residual anatase phase only for the powder sample treated at lower temperature.

Based on a thorough analysis of the spectrum (Fig. 4a) of the starting TiO_2-anatase powder, it is possible to observe the presence of the main active modes related to the anatase structure. The most active Raman modes ($A_{1g}+2B_{1g}+3E_g$) can be

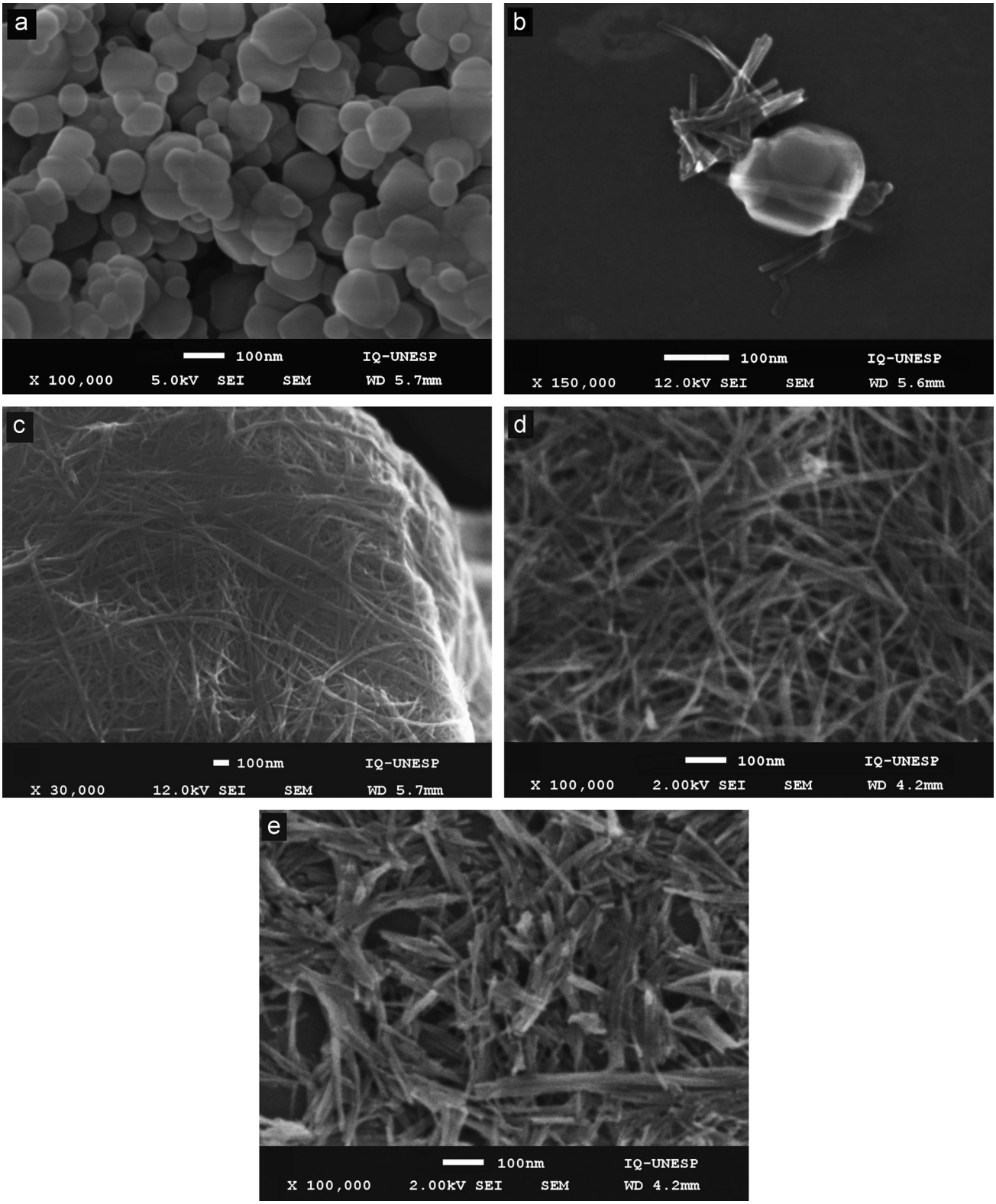

Fig. 2. SEM images of (a) TiO_2-anatase starting powder and powder samples obtained by MAH at (b) 130 °C for 2 h, (c) 130 °C for 4 h, (d) 150 °C for 1 h and (e)150 °C for 4 h.

visualized, and according to the results published by Ohsaka et al. [31], the active modes are located at 639 cm^{-1} (E_g,ν_1), 519 cm^{-1} (B_{1g}, ν_2), 513 cm^{-1} (A_{1g}, ν_3), 399 cm^{-1} (B_{1g}, ν_4), 197 cm^{-1} (E_g, ν_5) and 144 cm^{-1} (E_g, ν_6) as a result of the crystal structure composed of two TiO_2 formula unit per cell, where the titanium atom is centered onto oxygen atoms octahedron.

The results found for the short time treated samples, such as 130 ºC for 2 h and 150 ºC for 1 h (Fig. 4) led to the presence

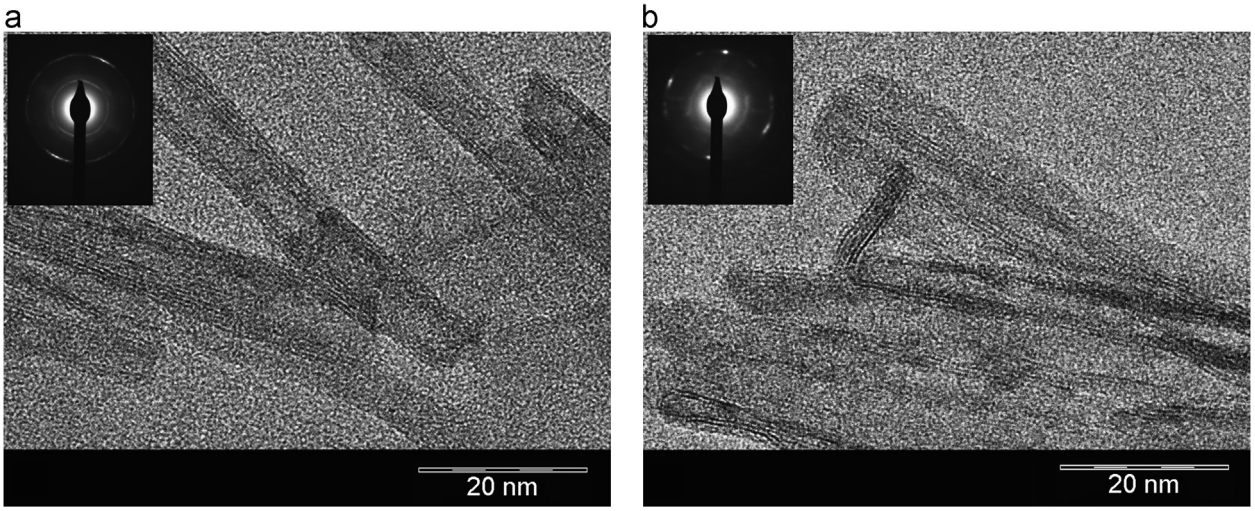

Fig. 3. TEM images of samples obtained from MAH for 4 h at (a) 130 °C and (b) 150 °C. The inset figures show for each sample the electron diffraction pattern.

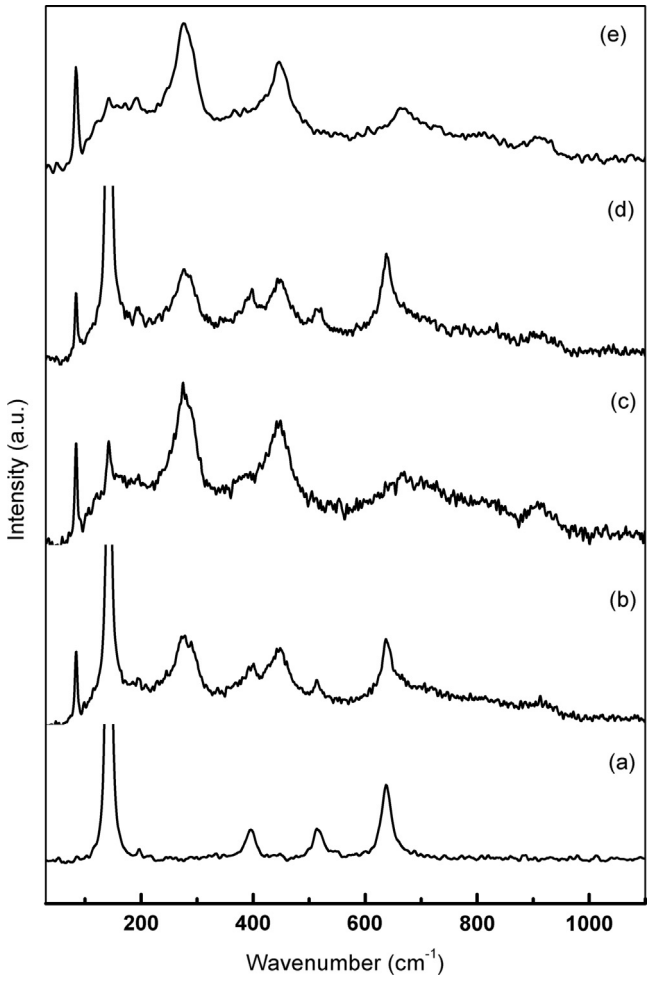

Fig. 4. Raman spectra of (a) TiO_2-anatase and the samples (b) 130 °C for 2 h, (c) 130 °C for 4 h, (d) 150 °C for 1 h and (e) 150 °C for 4 h obtained by MAH.

of intense peaks associated to the active modes of anatase and nanotube structures that coexist in considerable amount, confirming the results detectable by XRD and SEM analyses (Figs. 1 and 2). Besides that, the peaks around 280 cm^{-1} and

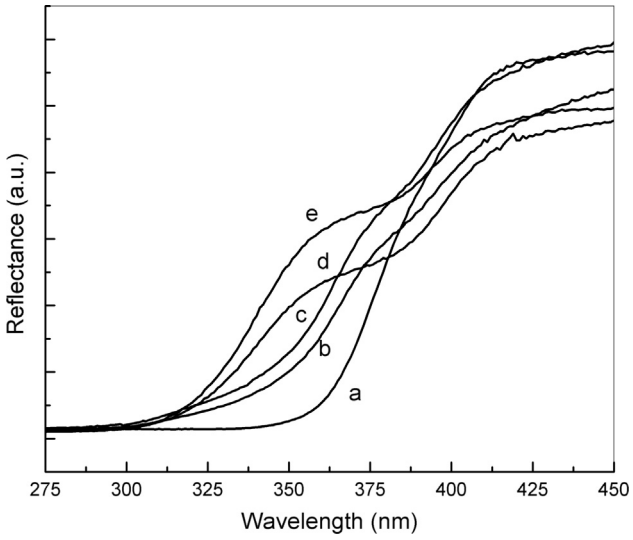

Fig. 5. Diffuse UV–vis reflectance spectra for (a) TiO_2-anatase and samples obtained by MAH at several reaction conditions: (b) 150 °C for 1 h, (c) 130 °C for 2 h, (d) 130 °C for 4 h and (e) 150 °C for 4 h.

660 cm^{-1}, associated to Na–O–Ti bonds [7], and other peaks, such as the one at 911 cm^{-1}, related to Ti–O terminal bond [32], indicate that some defects are present due to network distortions related to the curvature of the nanotube wall, breaking the long range ordering. However, the remaining peaks related to E_g,ν_1 and E_g,ν_6 active modes indicate that the TiO_6 octahedral vibration is also present in the sodium titanate nanotube structure, mainly the vibrational mode at 141.5 cm^{-1} [21]. This fact indicates that the nanotubes are formed by rearrangement of TiO_6^{2-} octahedrons in order to convert long range ordered structure of tetragonal anatase phase into a short range ordered nanotube structure.

The powder samples were analyzed by diffuse UV–vis reflectance spectroscopy and the results are shown in Fig. 5. The typical profile for anatase structure visualized in the spectrum (Fig. 5a) is altered proportionally to the nanotube

amount in the powder samples. This event is time dependent (by comparing *b* and *e* spectra), but the temperature of the treatment also affects the profile changing (by comparing *d* and *e* spectra), as a result of the different reaction rates in the different temperatures. The nanotube presence is marked by the formation of a shoulder in the uptake curves in the UV-A region (from 320 to 400 nm) [33,34].

Given that the observed reduction of the absorption in UV-A region is occurring due to the sodium titanate nanotube formation, which is followed by a reduction in the long range ordering of anatase phase, it can be that the main cause for UV-A absorption is related to the anatase crystalline structure. The fact that the anatase and rutile structures possess different absorption region edges, as reported in the literature backs this hypothesis. According to a previous work [35], the appearance of this shoulder as a response to the nanotube formation is related to the intermediate state rising between conduction and valence bands, as a consequence of the structural disordering process associated to the nanotube formation.

The band gap energy for the main edge absorption for all the samples is shown in Table 1. It can be observed that the $Na_2Ti_6O_{13}$-nanotubes structure possesses higher band gap energy compared to the anatase ones. These increases in band-gap energy are correlated with the material structural modification, since there was a complete conversion of TiO_2-anatase on $Na_2Ti_6O_{13}$-nanotubes. The DRX pattern showed that for the temperature 130 °C, Fig. 1a, after 2 h of reaction two phases are found to coexist (TiO_2 and $Na_2Ti_6O_{13}$), thereby the curve showed at UV–vis spectrum (Fig. 5c) is the contribution of these two crystalline phases. Increasing the reaction time for 4 h at the same temperature leads to a different profile on UV–vis spectrum (Fig. 5d) with the presence of a shoulder, characteristic of the nanotubes structure, which corresponds to a secondary band gap value.

All of the powder samples were characterized by photoluminescence spectroscopy, as shown in Fig. 6. By shifting the main emission peak from 548.5 nm, associated to the anatase starting powder, to 524 nm associated to the sample containing nanotube single phase with thin wall (130 ºC for 4 h), it can be concluded that the titanate nanotubes structures have profound defects like oxygen vacancies that lead to high energy emission (violet and blue region). The Electrons Difraction Pattern (Fig. 3) showed low crystallinity structures for these samples which corroborate this behavior. On the other hand the sample obtained at 150 °C for 4 h which has crystalline and thicker wall, the emission peak shifted to lower energy

Table 1
Band gap results for samples obtained by MAH for varying synthesis time and temperature.

Sample	λ (nm)	E_{gap} (eV)
TiO_2-anatase	359.5	3.45
150 °C/1 h	339.5	3.65
130 °C/2 h	335.9	3.69
130 °C/4 h	317.8 (shoulder in 380.5)	3.90 (3.25 for shoulder)
150 °C/4 h	316.7 (shoulder in 380.6)	3.91 (3.25 for shoulder)

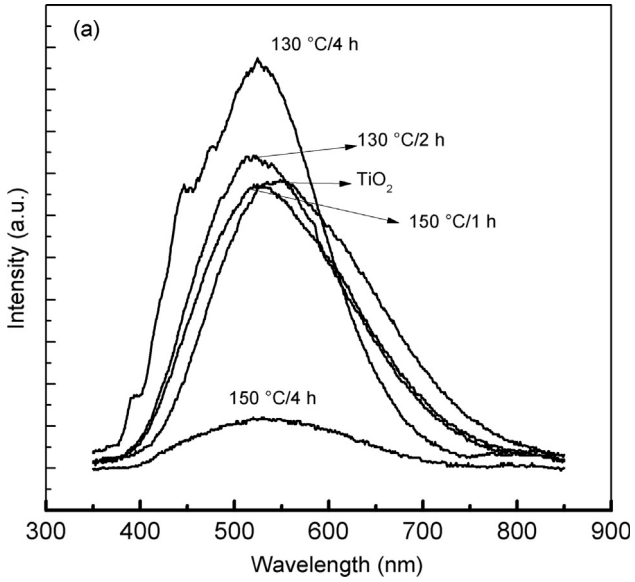

Fig. 6. Photoluminescence spectra acquired from the powders TiO_2-anatase, and obtained by MAH at 130 °C for 2 h, 130 °C for 4 h, 150 °C for 1 h, 150 °C for 4 h.

(531 nm) indicating the presence of clusters distortions, known as surface defects lead to lower energy emission (green, yellow and red region) [23].

Photoluminescence measurements presented in Fig. 6 were performed with the same experimental conditions and sequentially on the same date, so it is possible to qualitatively compare these intensities. The PL intensity emission peak for samples obtained at 130 °C for 2 h and 150 °C for 1 h, which present both phases nanotubes and TiO_2-anatase, is similar to starting material. However the PL intensities for nanotubes single phases are quite different according to the synthesis temperature. The sample obtained at 130 °C for 4 h has the higher intensity on the other hand the sample obtained at 150 °C has the lowest emission intensity. This behavior was found to be related to the covering of the nanotube by a more organized structure, thus making the nanotube wall thicker while attenuating the emission peak associated to the nanotube structure. Hence it is worthy to point out that the emission peak for a thick wall structure (150 °C for 4 h) occurs at a wavelength (531 nm) higher than that observed for the samples with thin wall (150 ºC for 1 h or 130 ºC for 4 h). The mechanism related to the internal stress reduction due to the cool shrinkage effect can undoubtedly explain this outcome [36].

The emission peak intensities appear to be proportional to the rate of the recombination of the photogenerated electrons and correspondent holes. However, when the structure has lower defect concentration acting as electron trap centers, the emission peak intensity tends to decrease as well [37]. Although photoluminescence peak emission can be reduced by surface or structural defects reduction due to longer hydrothermal treatment [23], the most probable hypothesis is that a thicker wall attenuates the effect of the several microstrains, such as oxygen vacancies and structural distortions existent in the inner wall. The thicker outside wall exhibits higher degree of crystallinity, besides the lower concentration of defects.

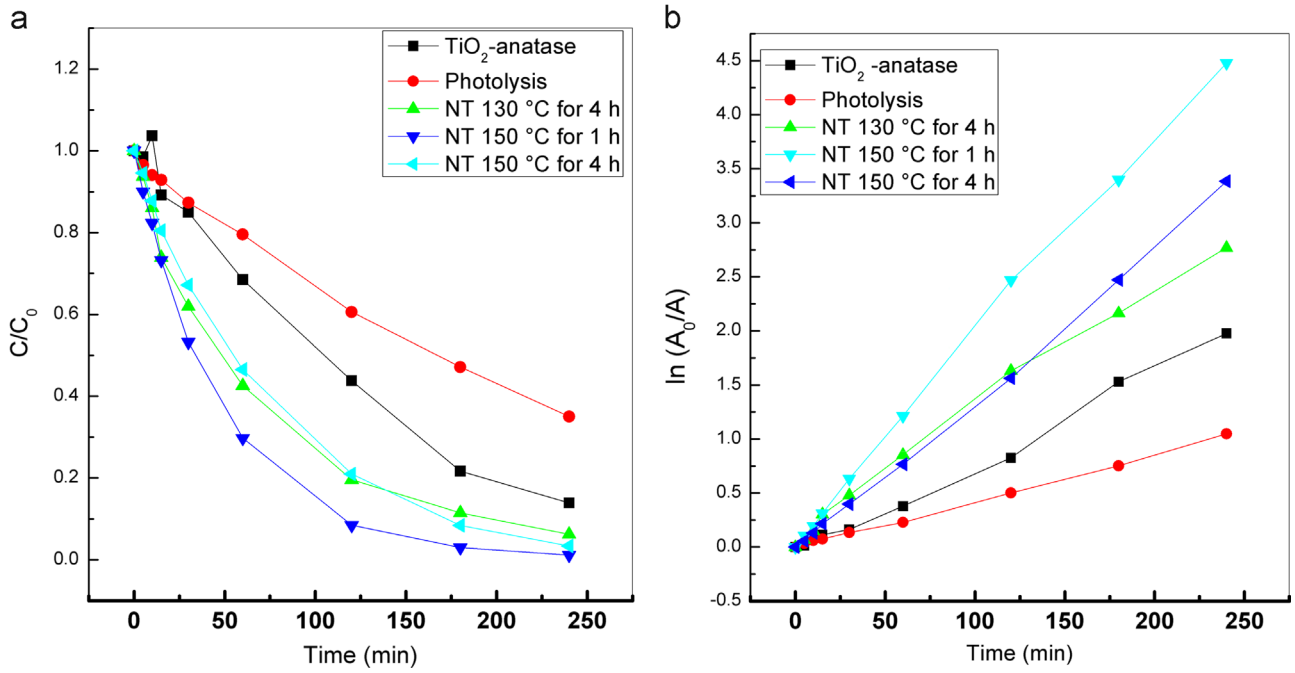

Fig. 7. Photocatalytic studies of rhodamine-B degradation under UV irradiation of TiO_2-anatase and titanate nanotubes obtained from MAH. (a) Relative concentration curves and (b) kinetic study.

Fig. 7a displays the time-dependence decolorization of rhodamine-B over nanotubes prepared at different temperatures and time. No significant rhodamine-B photodegradation has occurred in the absence of catalysts under commercial germicide lamps irradiation for 4 h. An interesting finding is that the smaller particle size of catalysts (nanotubes) increases the photocatalysts activities. After 240 min illumination, the rhodamine-B decolorization reached 87% for TiO_2-anatase (starting phase), 93.7% for nanotubes synthesized at 130 °C for 4 h, 96.6% for nanotubes obtained at 150 °C for 4 h and 96.9% for nanotubes obtained at 150 °C for 1 h.

The degradation rate could be obtained by plotting the natural logarithm of the absorbance against irradiation time, Fig. 7b. It could be observed that the nanotubes obtained at 150 °C for 1 h has faster decolorization of rhodamine-B with decolorization's rate 0.01879 min^{-1}. The average decomposition rate of all of samples, under 290 nm irradiation was 0.00425 min^{-1} for photolysis, 0.00837 min^{-1} for TiO_2-anatase, 0.01158 min^{-1} for sample 130 °C for 4 h, 0.01394 min^{-1} for sample 150 °C for 4 h. In this study, we reported that structural and morphological transformations of TiO_2-anatase in sodium titanate nanotubes (with a monoclinic $Na_2Ti_6O_{13}$ structure) promote the improvement of photocatalysts activities of samples under UV-light.

4. Conclusion

In this study, the microwave hydrothermal method was used to synthesize sodium titanate nanotubes with a monoclinic $Na_2Ti_6O_{13}$ structure. The TiO_2-anatase phase used as the starting powder is totally consumed by the dissolution–reprecipitation process at different time depending on the synthesis temperature. However, the Raman measurement indicates that the octahedron titanium centered is the base of the new structure. It was noted that the nanotubes size is about micrometers of length and their outer diameters are found to be affected by reaction time and temperature, 11 nm (130 °C for 4 h) and 20 nm (150 °C for 4 h). For the higher temperature there is an improvement in crystallinity, but they have the same crystalline structure. The high disordered nanotube structure is a result of some defects as oxygen vacancies and clusters distortions, which affect the electronic properties, such as photoluminescence and band gap energy, also the improvement on photocatalysis activity was observed for these titanate nanotubes.

Acknowledgments

We would like to express our gratitude and indebtedness to the LMA-IQ for providing the TEM and FEG-SEM facilities. We would like to acknowledge CAPES, FAPESP (No. 2013/07296-2) and CNPq (No. 482943/2012-2) for financial support.

References

[1] M. Hua, S. Zhang, B. Pan, W. Zhang, L. Lv, Q. Zhang, Heavy metal removal from water/wastewater by nanosized metal oxides: a review, J. Hazard. Mater. 211–212 (2012) 317–331.
[2] H. Jamil, S.S. Batool, Z. Imran, M. Usman, M.A. Rafiq, M. Willander, M.M. Hassan, Electrospun titanium dioxide nanofiber humidity sensors with high sensitivity, Ceram. Int. 38 (2012) 2437–2441.
[3] J. Xi, N.A.L. Dahoudi, Q. Zhang, Y. Sun, G. Cao, Effect of annealing temperature on the performances and electrochemical properties of TiO_2 dye-sensitized solar cells, Sci. Adv. Mater. 7 (2012) 727–733.
[4] A. Liu, M. Wei, I. Honma, H. Zhou., Biosensing properties of titanatenanotube films: selective detection of dopamine in the presence of ascorbate and uric acid, Adv. Funct. Mater. 16 (2006) 371–376.

[5] A.R. Malagutti, H.A.J.L. Mourão, J.R. Garbin, C. Ribeiro, Deposition of TiO_2 and Ag:TiO_2 thin films by the polymeric precursor method and their application in the photodegradation of textile dyes, Appl. Catal. B – Environ., 90, , 2009, p. 205–212.
[6] W. Huang, F. Wang, W. Wang, Fabrication of TiO_2 colloidal crystal films and characterization of their photocatalytic properties, J. Nanoeng. Nanomanuf. 3 (2011) 265–271.
[7] D. Singh, S. Kumar, S.C. Singh, B. Lal, N.B. Singh, Applications of liquid assisted pulsed laser ablation synthesized TiO_2 nanoparticles on germination, growth and biochemical parameters of *Brassica oleracea* var, Capit. Sci. Adv. Mater. 3-4 (2012) 522–531.
[8] C. Moseke, F. Hage, E. Vorndran, U. Gbureck, TiO_2 nanotube arrays deposited on Ti substrate by anodic oxidation and their potential as a long-term drug delivery system for antimicrobial agents, Appl. Surf. Sci. 258 (2012) 5399–5404.
[9] A.-L. Papa, L. Dumont, D. Vandroux, N. Millot, Titanate nanotubes: towards a novel and safer nanovector for cardiomyocytes, Nanotoxicology 7 (2013) 1131–1142.
[10] J. Wang, J. Sun, X. Bian, Preparation of oriented TiO2 nanobelts by microemulsion technique, Mat. Sci. Eng. A – Struct. 379 (2004) 7–10.
[11] A.A.S. Alfaya, L.T. Kubota., A utilização de materiais obtidos pelo processo de sol–gel na construção de biossensores, Quím. Nova 25 (2002) 835–841.
[12] L. Perazolli, L. Nuñez, M.R.A. da Silva, G.F. Pegler, A.G.C. Costalonga, R. Gimenes, M.M. Kondo, M.A.Z. Bertochi., TiO_2/CuO films obtained by citrate precursor method for photocatalytic application, Mater. Sci. Appl. 2 (2011) 564–571.
[13] R. Savua, R. Parraa, E. Joanni, B. Jancar, S.A. Eliziario, R. de Camargo, P.R. Bueno, J.A. Varela, E. Longo, M.A. Zaghete, The effect of cooling rate during hydrothermal synthesis of ZnO nanorods, J. Cryst. Growth 311 (2009) 4102–4108.
[14] E.M. Nevillea, J.M.D. MacElroy, K.R. Thampi, J.A. Sullivan, Visible light active C-doped titanate nanotubes prepared via alkaline hydrothermal treatment of C-doped nanoparticulate TiO_2: photo-electrochemical and photocatalytic properties, J. Photochem. Photobiol. A 267 (2013) 17–24.
[15] C.-C. Hu, T.-C. Hsu, S.-Y. Lu, Effect of nitrogen doping on the microstructure and visible light photocatalysis of titanate nanotubes by a facile cohydrothermal synthesis via urea treatment, Appl. Surf. Sci. 280 (2013) 171–178.
[16] I.A. Santos-López, B.E. Handy, R. García-de-León, Titanate nanotubes as support of solid base catalyst, Thermochim. Acta 567 (2013) 85–92.
[17] D.L. Morgan, H.-Y. Zhu, R.L. Frost, E.R. Waclawik, Determination of a morphological phase diagram of titania/titanate nanoestructures from alkaline hydrothermal treatment of Degussa P25, Chem. Mater. 20 (2008) 3800–3802.
[18] T. Kasuga, M. Hiramatsu, A. Hoson, T. Sekino, K. Niihara, Formation of titanium oxide nanotube, Langmuir 14 (1998) 3160–3163.
[19] T. Kasuga, M. Hiramatsu, A. Hoson, T. Sekino, K. Niihara, Titania nanotubes prepared by chemical processing, Adv. Mater. 11 (1999) 1307–1311.
[20] C.-C. Tsai, J.-N. Nian, H. Teng, Mesoporous nanotube aggregates obtained from hydrothermally treating TiO_2 with NaOH, Appl. Surf. Sci. 253 (2006) 1898–1902.
[21] L.-Q. Weng, S.-H. Song, S. Hodgson, A. Baker, J. Yu, Synthesis and characterisation of nanotubular titanates and titania, J. Eur. Ceram. Soc. 26 (2006) 1405–1409.
[22] K. Kiatkittipong, J. Scott, R. Amal, Hydrothermally synthesized titanate nanostructures: impact of heat treatment on particle characteristics and photocatalytic properties, ACS Appl. Mater. Interfaces 3 (2011) 3988–3996.
[23] J. Huang, Y. Cao, Z. Deng, H. Tong, Formation of titanate nanostructures under different NaOH concentration and their application in wastewater treatment, J. Solid State Chem. 184 (2011) 712–719.
[24] C.-C. Chung, T.-W. Chung, T.C.-K. Yang, Rapid synthesis of titania nanowires by microwave-assisted hydrothermal treatments, Ind. Eng. Chem. Res. 47 (2008) 2301–2307.
[25] Y.-P. Peng, S.-L. Lo, H.-H. Oua, S.-W. Lai, Microwave-assisted hydrothermal synthesis of N-doped titanate nanotubes for visible-light-responsive photocatalysis, J. Hazard. Mater. 183 (2010) 754–758.
[26] D. Liu, T. Liu, C. Lv, W. Zeng, Hydrothermal synthesis and gas sensing properties of different titanate nanostructures, J. Mater. Sci. – Mater. Electron. 23 (2012) 576–581.
[27] M.H. Razali, A.-F.M. Noor, A.R. Mohamed, S. Sreekanta, Morphological and structural studies of titanate and titania nanostructured materials obtained after heat treatments of hydrothermally produced layered titanate, Corp. J. .Nanomater 2012 (2012) 10 (Article ID 962073).
[28] S.K. Pradhan, Y. Mao, S.S. Wong, P. Chupas, V. Petkov Atomic-Scale, Structure of nanosized titania and titanate: particles, wires, and tubes, Chem. Mater. 19 (2007) 6180–6186.
[29] S. Ribbens, V. Meynen, G. Van Tendeloo, X. Ke, M. Mertens, B.U. W. Maes, P. Cool, E.F. Vansant, Development of photocatalytic efficient Ti-based nanotubes and nanoribbons by conventional and microwave assisted synthesis strategies, Microporous Mesoporous Mater. 114 (2008) 401–409.
[30] R.A. Zárate, S. Fuentes, A.L. Cabrera, V.M. Fuenzalida, Structural characterization of single crystals of sodium titanate nanowires prepared by hydrothermal process, J. Cryst. Growth 310 (2008) 3630–3637.
[31] T. Ohsaka, Temperature dependence of Raman spectrum in anatase TiO_2, J. Phys. Soc. Jpn. 48 (1980) 1661–1668.
[32] B.C. Viana, O.P. Ferreira, A.G. Souza Filho, A.A. Hidalgo, J. Mendes Filho, O.L. Alves, Highlighting the mechanisms of the titanate nanotubes to titanate nanoribbons transformation, J. Nanopart. Res. 13 (2011) 3259–3265.
[33] F.R.C. Ciaco, F.M. Pontes, C.D. Pinheiro, E.R. Leite, S.R. de Lazaro, J.A. Varela, P.S. Pizani, C.A. Paskocimas, A.G. Souza, E. Longo, O papel dos modificadores de rede na produção da fotoluminescência no $CaWO_4$, Cerâmica 50 (2004) 43–49.
[34] P.R. de Lucena, F.M. Pontes, C.D. Pinheiro, E. Longo, P.S. Pizani, S. L.ázaro, A.G. Souza, I.M.G. dos Santos, Fotoluminescência em materiais com desordem estrutural, Cerâmica 50 (2004) 138–144.
[35] G.F. Teixeira, M.A. Zaghete, G. Gasparotto, M.G.S. Costa, J.W.M. Espinosa, E. Longo, J.A. Varela, Photoluminescence properties and synthesis of a PZT mesostructure obtained by the microwave-assisted hydrothermal method, J. Alloys Compd. 512 (2012) 124–127.
[36] L.Z. Liu, W. Xu, X.L. Wu, Y.Y. Zhang, T.H. Chen, P.K. Chu, Electronic states and photoluminescence of TiO_2 nanotubes with adsorbed surface oxygen, Appl. Phys. Lett. 100 (2012) 121904.
[37] X. Yang, C. Cao, L. Erickson, K. Hohn, R. Maghirang, K. Klabunde, Synthesis of visible-light-active TiO_2-based photocatalysts by carbon and nitrogen doping, J. Catal. 260 (2008) 128–133.